ADVANCED MATERIALS TECHNOLOGIES
www.advmattechnol.de

Utilization of Synergistic Effect of Dimension-Differentiated Hierarchical Nanomaterials for Transparent and Flexible Wireless Communicational Elements

Xiao Sun, Houfang Liu, Haochuan Qiu, Xiufeng Jia, Yiheng Ma, Kaihui Liu, Jierui Yu, Dongdong Hu, Congwei Tan, Fang Yi, Jun Fu, Hailin Peng, Di Wei, Tian-Ling Ren,* and Zhongfan Liu**

The demand of emerging transparent and flexible wireless electronic devices is ever-increasing for Internet of Things (IoT) scenarios, like noninvasive healthcare, real-time wearable electronics, etc. However, as an essential part of the IoT wireless communicational devices, radio frequency (RF) antennas are still hampered by poor-flexibility, low-conductivity, and weak-transparency. Here, based on the unique electronic and optical properties of graphene, a method to obtain these appealing features concurrently through promoting synergistic effect between two-dimensional (2D) and one-dimensional (1D) materials is studied. It is found that this method could not only successfully maintain transparency and flexibility, but also greatly enhance the overall performance of the antenna. The fabricated antenna exhibits a 75% light transmittance, from 5.6 to 12.8 GHz ultrawide bandwidth and outstanding durability and stability. Moreover, a transparent and flexible radio frequency identification (RFID) tag is also designed and demonstrated with a remarkable reading distance. These findings show that the method by promoting synergistic effect of hybrid materials has great potential in the design of next generation novel and high-performance wireless electronics.

1. Introduction

Internet of Things (IoT) has been treated as one of the trending technologies in recent years. Wireless communicational device as an essential part of the IoT network has attracted much attention in many areas such as wearable applications. Fully optical transparency becomes one of the necessities for these devices, e.g., a recent study reported an under-screen transparent antenna array, which was utilized in the assembly of next-generation cellphones.[1] The real-time noninterruptive transparent and flexible wireless communicational devices are needed in a wide range of scenarios. For example, transparency is in exact need in applications such as smart contact lenses for not blocking the user's vision while enabling the noninvasive method for continuous medical diagnosis.[2,3] Furthermore, on top of transparency, flexibility is also a very important ingredient, especially for wearable devices. Excellent flexibility of such wireless electronics is also necessary in order to closely match the curvature of the eyeballs, reducing the discomfort of patients.[4] To fabricate transparent and flexible wireless devices, the main challenge remains the realization of transparent and flexible antenna. Therefore, the demand of transparent and flexible antenna has been rapidly growing in recent years.

Dr. X. Sun, Y. Ma, Prof. K. Liu, C. Tan, Prof. F. Yi, Prof. H. Peng, Prof. Z. Liu
Center for Nanochemistry
Beijing Science and Engineering Center for Nanocarbons
Beijing National Laboratory for Molecular Sciences
College of Chemistry and Molecular Engineering
Peking University
Beijing 100871, P. R. China
E-mail: zfliu@pku.edu.cn

Dr. X. Sun, C. Tan, Prof. H. Peng, Prof. Z. Liu
Academy for Advanced Interdisciplinary Studies
Peking University
Beijing 100871, P. R. China

The ORCID identification number(s) for the author(s) of this article can be found under https://doi.org/10.1002/admt.201901057.

DOI: 10.1002/admt.201901057

Dr. H. Liu, H. Qiu, X. Jia, Prof. J. Fu, Prof. T.-L. Ren
Institute of Microelectronics and Beijing National Research Center for Information Science and Technology (BNRist)
Tsinghua University
Beijing 100084, China
E-mail: rentl@tsinghua.edu.cn

Prof. K. Liu
State Key Laboratory for Mesoscopic Physics
School of Physics
Peking University
Beijing 100871, China

J. Yu
Department of Chemistry and Biochemistry
Southern Illinois University
1245 Lincoln Drive, Carbondale, IL 62901, USA

D. Hu, Prof. H. Peng, Dr. D. Wei, Prof. Z. Liu
Beijing Graphene Institute (BGI)
Beijing 100094, P. R. China
E-mail: weidi-cnc@pku.edu.cn

Unlike transparent and flexible screens,[5] batteries[6] and circuits,[7] which have been increasingly investigated over the past decade, a transparent and flexible antenna for wireless electronics remains as an underdeveloped topic. Conventional commercial antennas are mainly made by plain metals, alloys or nanoparticles, such as silver, copper or aluminum.[8–10] There are many limitations of these metallic antennas, such as low transparency and easily being corroded or oxidized. Additionally, a drastic change in impedance occurs when such an antenna is bent or folded, resulting in the loss of communication efficacy. The ability to tolerate shape changes is vital for wearable flexible electronics, as movement of the body and wrinkling of clothes easily lead to shape changes of attached antennas, thus degrading the performance of the antenna.[11,12] To satisfy the needs of flexibility and transparency, high electrical conductivity and stability of the antenna should also be taken into consideration. From this aspect, the fabrication of flexible and transparent antenna with high performance is very difficult. New efforts using conductive polymers,[13] carbon nanotubes,[14–16] printed graphene paper/ink,[17–19] MoS_2[20] and 2D MXene[21] have been made to produce flexible and transparent antennas. However, their poor conductivity and low transparency are still hindering the performance and potential applications of these antennas.

Graphene has been proven to exhibit attractive electronic and optical properties due to its sp^2 orbital hybridization and linear dispersion of massless Dirac fermions. This atoms-thick material shows excellent transmittance of light as high as 97.7%, extremely high carrier mobility with theoretically 200 000 cm^2 V^{-1} s^{-1} at room temperature and mechanical robustness with intrinsic tensile strength of 130 GPa and Young modulus of 1 TPa.[22–24] Besides, due to its flexibility, monolayer graphene film can be bent or even folded.[25] Dense electronic cloud allows perfect graphene film to be impermeable to all atoms and molecules under ambient conditions, even hydrogen, making it an effective anticorrosion coating.[26,27] Furthermore, graphene's ultrahigh carrier mobility brings it great potential for radio frequency applications. All of these properties underline that graphene can be considered as a highly competitive material for flexible and transparent antenna.

Herein, we demonstrate a method for the first fully optically transparent and flexible antenna of real-time communication by promoting the synergistic effect between graphene and silver nanowires (AgNW) when designing and fabricating the devices. The wireless communicational element showed good light transmittance, ultrawide frequency band performance, excellent flexibility, and high reliability. Meanwhile, as a critical demonstration, a fully optically transparent and flexible ultra-high-frequency RFID antenna coupled with integrated circuit (IC) chips was fabricated and tested by a portable RFID reader system.

2. Results and Discussion

High flexibility and transparency would greatly broaden the applications of wireless electronics in the future (**Figure 1**a, for the electromagnetic spectrum and applications in communication technologies see Notes S1 and S2, Supporting Information). After consideration, a nanomaterial composite graphene/AgNW/ethylene vinyl acetate/polyethylene terephthalate laminated film (graphene/AgNW/EVA/PET)[28] was chosen among all candidates for the fabrication of flexible and transparent antennas for wireless electronics. The composite was composed of a uniform monolayer graphene film laminated on top of the AgNW network layer precoated on the EVA side of an EVA/PET double-layered substrate, as demonstrated in Figure 1b. The graphene used for the antenna composite film was high-quality

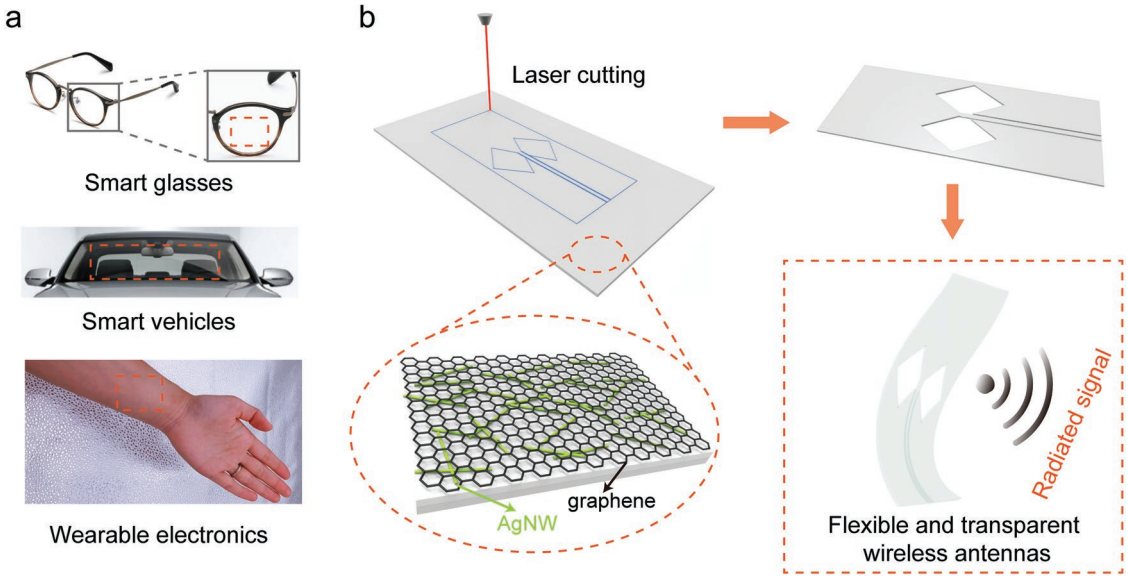

Figure 1. Schematic of the fabrication process and future applications of graphene/AgNW-based flexible and transparent antennas. a) Future applications of flexible and transparent wireless electronics, such as being a key component of smart glasses, smart vehicles or wearable electronics. b) Laser cutting of graphene/AgNW/EVA/PET laminated film to shape the antenna. Notably, the antenna based on the graphene/AgNW/EVA/PET film is bendable and nonopaque and can thus be used for flexible and transparent wireless communicational antennas.

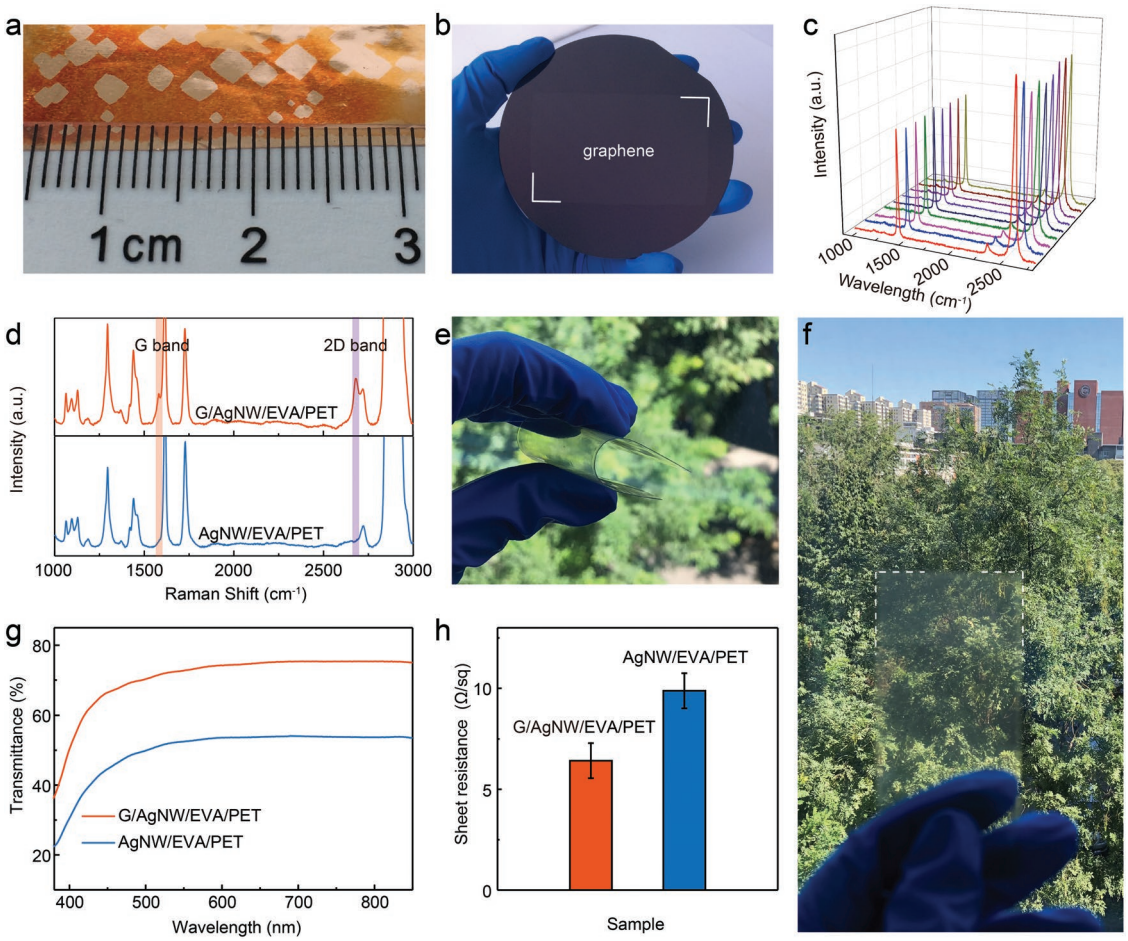

Figure 2. Characterization of graphene and hybrid films for antennas. a) Photograph of CVD-grown graphene domains with 2 mm diameter. These graphene domains on copper foil became visible after heating in air for 5 min at 200 °C. b) Photograph of the continuous graphene film transferred onto a 4 in. SiO_2/Si wafer. c) Raman spectra of the large single-crystalline graphene film. d) Raman spectra of graphene/AgNW/EVA/PET film and AgNW/EVA/PET film. The characteristic G band and 2D band of graphene are clearly shown. The letter "G" represents graphene. The graphene/AgNW/EVA/PET film is e) flexible and f) highly transparent. g) Transparency comparison of film graphene/AgNW/EVA/PET and AgNW/EVA/PET. h) Sheet resistances of graphene/AgNW/EVA/PET and AgNW/EVA/PET, which were averaged from 40 randomly selected places on each film, with error bars.

uniform monolayer graphene film with domain size of ≈2 mm (**Figure 2**a–c, growth method[29] see Note S3, Supporting Information). Through hot lamination and electrochemical bubbling delamination,[28] the composite film graphene/AgNW/EVA/PET was successfully obtained (details see Note S4 and Figure S1, Supporting Information). Related Raman characterizations were conducted for AgNW/EVA/PET and graphene/AgNW/EVA/PET films. Graphene peaks are explicitly labeled in Figure 2d. Characteristic G and 2D bands (≈1582 cm^{-1} and ≈2681 cm^{-1}, respectively) and almost negligible D band of graphene indicated graphene was successfully transferred onto AgNW/EVA/PET without damage.[30,31] The graphene/AgNW/EVA/PET laminated film shows excellent flexibility and can thus be easily bent (Figure 2e). Interestingly, the laminated film shows great light transmittance of ≈75% (Figure 2f,g), which is much higher than bare AgNW/EVA/PET without graphene. The improvement in transmittance mainly results from the melting and resolidification of EVA during the hot lamination process, which makes EVA more permissive to light transmittance. Therefore, although monolayer graphene has a light absorption of 2.3%, the overall absorption is significantly decreased compared to the film without graphene. This method to promote film transparency is not valid for AgNW/EVA/PET films because hot lamination will drastically accelerate the oxidation rate of AgNW, meanwhile, the melted EVA will damage the hot-press machine without the protection of graphene.[28,32]

Besides, graphene/AgNW/EVA/PET film has better conductivity, with a sheet resistance of 6 Ω sq^{-1}, while that of the AgNW/EVA/PET film is ≈10 Ω sq^{-1} (Figure 2h). This reduction will lead less energy to be dissipated as heat.[33] The improvement in the conductivity may be due to the high carrier mobility of graphene, and in another aspect, graphene could improve the interconnection of the AgNW mesh through additional conductive channels across graphene grains. Furthermore, the existence of graphene over AgNW has been proven to improve the heat dissipation generated by the AgNW grid.[34] To prolong the lifespan of the antenna, the electrical conductivity of the material should be maintained at a desired level. The covering of graphene on the AgNW grid could effectively protect the NWs from being oxidized by either air or a more

oxidative environment (see Note S6, Figures S2 and S3, Supporting Information). The corrosion resistance of this material indicates that it can be used for antennas with high reliability.

The synergistic effects between dimension-differentiated materials, which were 2D graphene layer and 1D AgNW in this case, not only helped to overcome these intrinsic problems from poor corrosion resistance of AgNW and low overall conductivity of monolayer graphene film, but also made the composite suitable for transparent and flexible antenna. First, the introduction of graphene as a 2D functional material to AgNW network could change the conductive mode of the hybrid material from wire-based (1D) to plane-based (2D). Therefore, the electrical conductivity was further improved and the generated heat was reduced. It was important for the over-all impedance of the antenna to obtain a better compatibility with the integrated chip. Second, the graphene film could protect AgNW from corrosion, and its introduction enabled hot-pressing method, resulting in the submersion of AgNW into the substrate of EVA. Compared with traditional dimension-maintaining protection (e.g., jacket-type coating of 1D wires), this method appeared to be a dimension-raising protection as 2D protective layer introduced, thus promoting the integration between each component of a device without sacrificing their respective performances. The corrosion experiments conducted by using CH_4N_2S for drastic environment and air for mild environment (details see Note S6, Figures S2 and S3, Supporting Information) revealed that the resulted antenna had a better tolerance to chemical corrosion. It showed both improved electrical stability and better uniformity among different areas of antenna after corrosion. Third, as for a higher transparency, the coating of graphene enabled the hybrid material made by the hot-pressing technique, which further improved the transparency of the element, resulting in a better light transmittance of over 75% for the graphene/AgNW-based antenna. The implement of this technique was another expression of synergistic effect between components. This kind of synergistic effect exists widely among different combinations of dimension-differentiated materials, not limited only within AgNW and graphene. In this case, benefiting from the synergistic effect between the graphene layer and the AgNW grid, much higher electrical conductivity, more stability and better light transmittance could be realized, which is essential for a high performance, corrosion-resistant, long-life, fully optically transparent and flexible antenna of wireless communication.

Based on the laminated graphene/AgNW/EVA/PET film, after considering the proper dimensions of the coplanar waveguide (CPW) line and slots, we proposed the geometric structure of a bow-tie slot antenna (see Note S7 and Figure S4, Supporting Information). A schematic of the reflection coefficient experimental setup for the graphene/AgNW-based antenna is shown in **Figure 3**a. To evaluate the input power acceptance level of the antenna, i.e., reflection coefficient, the scattering parameter S_{11} was measured by a vector network analyzer (VNA). Importantly, an antenna used in wireless communication must provide a reflection coefficient less than −10 dB over its frequency bandwidth, that is, $|S_{11}| > 10$ dB, which indicates that more than 90% of the input power can be transmitted.[35] As shown in Figure 3b, the resonant frequency of the antenna occurs at 8.293 GHz, with the reflection coefficient of −19 dB. The bandwidth for $|S_{11}| > 10$ dB is from 5.6 to 12.8 GHz, which is matched within the range of ultrawide bandwidth from 3.1 to 10.6 GHz. To further

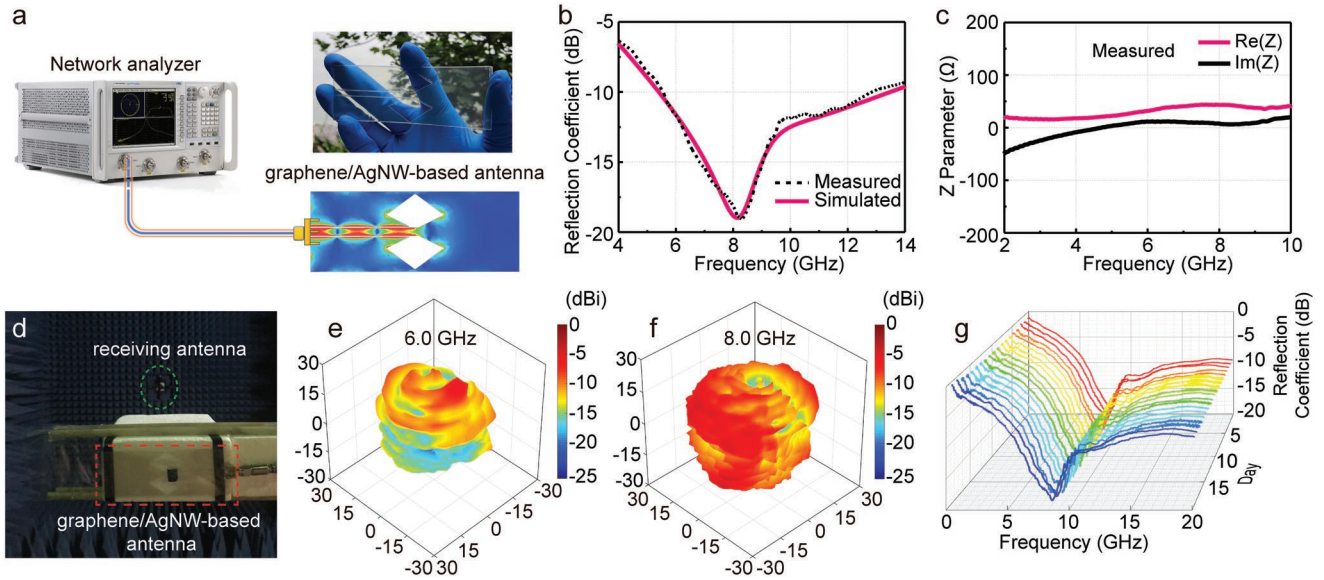

Figure 3. Graphene/AgNW-based antenna and its fundamental wireless performance. a) Schematic of the reflection coefficient measurement for the graphene/AgNW-based antenna. Inset: photograph of the antenna. b) Measured (dashed line) and simulated (solid line) reflection coefficients of the graphene/AgNW-based antenna. c) Measured *Z* parameter of the graphene/AgNW-based antenna. d) Photograph of the radiation pattern measurement setup in an anechoic chamber. A dual polarization horn antenna was used as the receiving antenna, whereas the tested antenna was the graphene/AgNW-based antenna. The black square in the middle of the antenna is double-sided tape used to fix the antenna. e,f) Experimental 3D normalized radiation patterns of the graphene/AgNW-based antenna at 6.0 and 8.0 GHz. Each plot center corresponds to −30 dBi. g) Reliability test of the graphene/AgNW-based antenna's reflection coefficients over the course of 20 days.

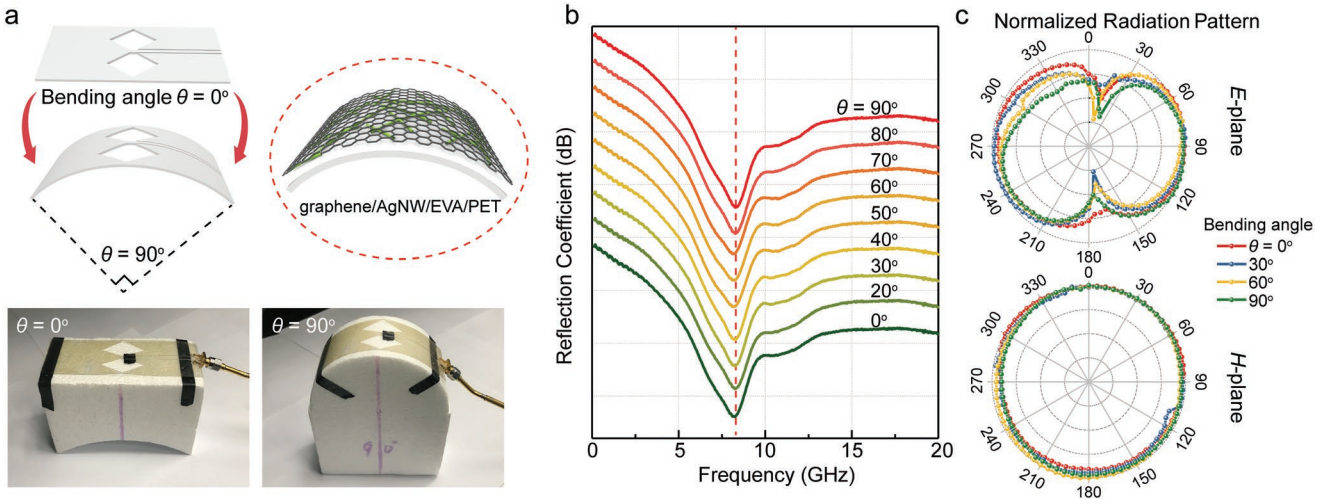

Figure 4. Bending characteristics of the graphene/AgNW-based antenna. a) Schematic and photographs of the bending test experimental setup for the graphene/AgNW-based antenna. The black strips (at the end) and squares (in the middle) in the figure are double-sided tape used to fix the antenna. b) Reflection coefficients and c) normalized E-plane and H-plane radiation patterns at 6.4 GHz of the graphene/AgNW-based antenna subjected to a series of bending angles ranging from 0° to 90°.

characterize the bandwidth of the antenna, the fractional bandwidth (FBW) can be defined as[36]

$$\mathrm{FBW} = (f_2 - f_1)/f_0 \tag{1}$$

where f_1 and f_2 are the lower and upper frequencies of the −10 dB bandwidth, respectively; f_0 is the resonant frequency of the antenna. The FBW of the graphene/AgNW-based antenna is calculated as 86.8%. Thus, this antenna can be referred to as an ultrawide band (UWB) antenna for wireless communication.

To characterize the graphene/AgNW-based antenna, an equivalent circuit model was proposed (see Note S8, Table S1, and Figure S5, Supporting Information). The simulation was performed with the Agilent advanced design system (Agilent ADS) based on the proposed equivalent circuit using parameters extracted from measurements. The reflection coefficient of the antenna in Figure 3b shows a good match between the simulation and measurement results. According to the S_{11} resonances, the input impedances can be precisely extracted for frequencies from 2 to 10 GHz (Figure 3c). The real and imaginary parts of the input impedance changed with increasing frequency, corresponding to the scanning curve on the Smith chart (Figure S6, Supporting Information). At resonance frequency f_0 = 8.293 GHz (S_{11} = −19 dB), the input impedance Z = 43.133 + 6.295j indicates that the fundamental resonance occurs at this frequency, and the graphene/AgNW-based antenna is well matched with only 1.2% of the input power reflected.

To further quantify the radiation properties, the normalized radiation patterns of the antenna were measured in an anechoic chamber (Figure 3d, Note S9 and Figure S7, Supporting Information). The 3D normalized radiation patterns at 6.0 GHz and 8.0 GHz are shown in Figure 3e,f (patterns for 2.4 GHz and 4.0 GHz are also provided in Figure S8a,b, Supporting Information). An approximately omnidirectional radiation pattern is observed in the H-plane for the 3D plot at 6.0 GHz, which is suitable for reliable wireless electronics in smart homes, and a nearly dipole-like radiation pattern in the E-plane appears, as expected (Figure S8c, Supporting Information). The long-term durability of the graphene/AgNW-based antenna over the course of 20 days was also explored through cyclic testing with daily measurement of the reflection coefficient. As shown in Figure 3g, the variation in S_{11} is almost negligible, implying good electrical reliability of the antenna against oxidation and corrosion, as expected.

For the flexibility test, the performance of the graphene/AgNW-based antenna was measured under different bending angles (Figures S9 and S10, Supporting Information). The bending angle was inversely proportional to the radius of the polystyrene mold. Note that the material of the mold did not affect the surface currents of the antenna. In **Figure 4**a, the antenna was measured at normal (0°) and bending (90°) angles and held by paper tape at the proper positions during measurements. As shown in Figure 4b, the reflection coefficients show neither changes nor degradation when the antenna is bent from 0° to 90°. In addition, the antenna was bent to 90° in a 1000 cycle test, with almost no degradation in performance (Figure S11, Supporting Information). Thus, the antenna shows great stability under different physical deformations. The normalized radiation patterns verify this result with almost no significant change (Figure 4c, Figures S12 and S13, Supporting Information).

To further evaluate the commercial potential of graphene/AgNW-based antennas, a functional, flexible, and transparent RFID tag assembled with an IC chip was designed, optimized, and fabricated, with an operating UHF band of 850–960 MHz (inset of **Figure 5**b and Figure S14, Supporting Information). The working principle[19,37,38] is presented in Figure 5a (details see Note S10, Supporting Information). The frequency dependence of the impedance of antennas from 850 to 960 MHz is illustrated in Figure S15 (Supporting Information), showing that in contrast with a pure AgNW-based antenna, the adhesion of graphene can greatly reduce the resistive component,

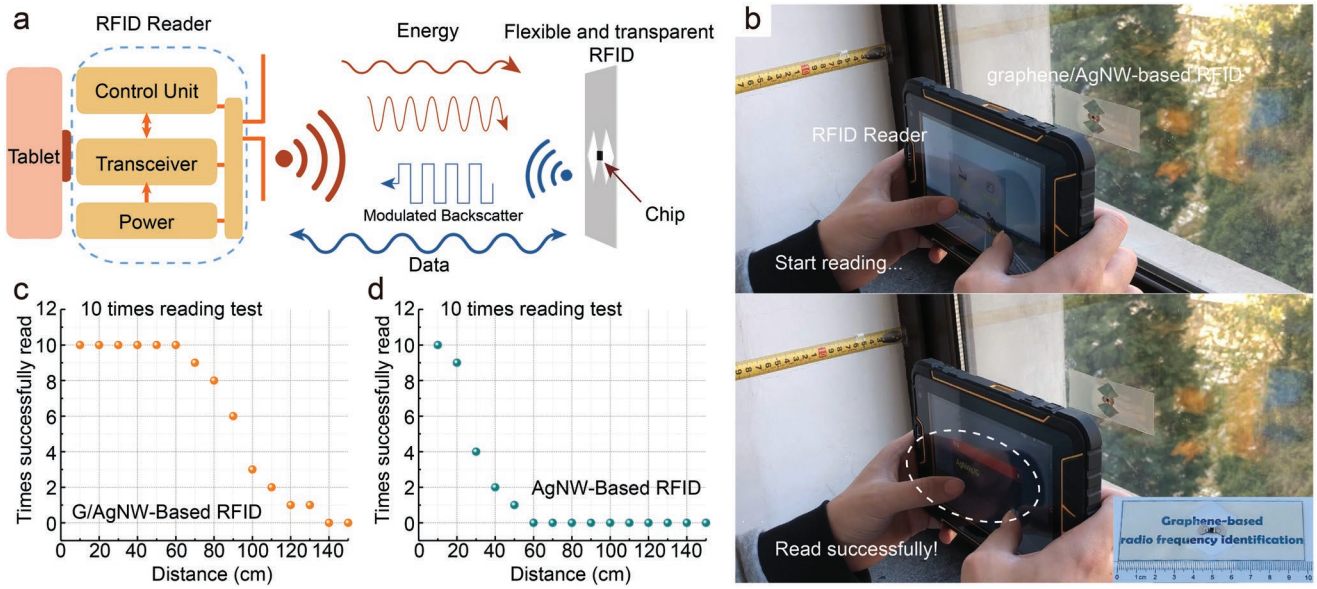

Figure 5. Working mechanism illustration and tests of flexible and transparent RFID tags. a) Working principle of RFID. The RFID transceiver (e.g., a reader) transmits energy to an RFID tag and reads the signal backscattered from it. b) The flexible and transparent graphene/AgNW-based RFID tag was tested with the RFID reader. An info box popping up immediately after clicking indicated that the tag was read successfully. The inset shows photograph of the graphene/AgNW-based tag. The times successfully read of c) graphene/AgNW-based and d) pure AgNW-based tags while the distance gradually increased. The reading tests were repeated 10 times at each distance.

improve the imaginary part of the whole impedance and further enhance the matching factor. The reading distances of graphene/AgNW-based and pure AgNW-based RFID tags were tested as a major reference factor. As one of the important parameters of RFID tags, the maximum activation range R_{max} can be expressed as[17,39]

$$R_{max} = (\lambda/4\pi)\sqrt{P_{tr}G_{read}G_{tag}\tau/P_{th}} \quad (2)$$

where λ is the carrier frequency wavelength; the product of P_{tr}-G_{read} is determined by the reader, where P_{tr} and G_{read} are the power transmitted by the reader and the gain of the reader antenna, respectively; G_{tag} is the gain of the tag antenna; P_{th} is the minimum threshold power to activate the tag chip; and τ is the transmission coefficient, which represents the matching level between the tag chip and the antenna. When the impedance of the antenna is equal to the complex conjugate of the impedance of the tag chip, maximum power transfer occurs, and $\tau = 1$. To improve the reading range, higher G_{tag} and τ are required for fixed λ, P_{tr}, G_{read}, and P_{th}. Thus, a larger reading distance stands for a better compatibility between chip and antenna, representing a better performance. At each distance, we tested the tags 10 times and recorded the times of successful reading (Figure 5c,d). The results reveal that the reading distance of the graphene/AgNW-based RFID tag could reach up to 130 cm, which is 2.6 times greater than that of the pure AgNW-based tag (50 cm).

Our work shows great improvement compared with other flexible and transparent antennas for wireless communication (**Table 1**), revealing that graphene/AgNW-based antennas are promising for potential application in E-skin, noninvasive healthcare monitoring, smart homes, flexible electronics and automobiles.

3. Conclusion

In conclusion, promoting the synergistic effect of 2D large single-crystalline graphene and 1D AgNW was demonstrated to be a brilliant way for the fabrication of flexible and transparent antenna, because it could not only maintain both transparency and flexibility but also greatly enhance the overall performance of the antenna. The graphene/AgNW-based antenna showed the light transmittance of over 75%. Excellent flexibility and physical deformation stability were also achieved with an almost negligible variation of reflection coefficients under different bending conditions and 1000 times bending test. Besides, the resulted antenna showed both good tolerance during the corrosion experiment and antiaging features in the long-term stability test. Graphene/AgNW-based RFID tag was fabricated with the reading distance of 130 cm, of which was much longer than an AgNW-based RFID tag, thanks to a better-matched impedance benefited from synergistic effect of graphene and AgNW. Our methodology on promoting the synergistic effect between 1D and 2D nanomaterials for highly reliable, flexible and transparent antennas will provide a new vision for the design of next-generation wireless electronics. More importantly, this method is also valid for a broader scope and appeals to a wide range of audience, as both 2D graphene and 1D AgNW can be substituted by other combinations of dimension-differentiated materials for other specific applications besides radiofrequency applications.

4. Experimental Section

Characterizations of Materials: Characterization was carried out using optical microscopy (Olympus BX51 optical microscope), SEM (Hitachi S4800 field-emission scanning electron microscope), UV–vis

Table 1. Comparison of the current flexible and transparent antennas for wireless communication.

Materials and structures	Transmittance	Flexible	Sheet Resistance [ohms sq^{-1}]@thickness	Frequency ($\|S_{11}\| > 10$ dB)	Demo device	Refs.
2D MXene	≈49%@62 nm ≈26%@114 nm	Yes	≈47@62 nm ≈20@114 nm	$f_0 \approx 2.4$ GHz@ 8000 nm	Yes	[21]
Graphene ink	–	Yes	–	3.8–15.5 GHz	Yes	[17]
Graphene nanoplatelets	–	Yes	0.19@62 000 nm	≈MHz	Yes	[19]
Graphene ink	–	Yes	–	3.75–12.88 GHz	–	[40]
Monolayer graphene	Yes	No	–	$f_0 \approx 20.7$ GHz	–	[41]
Ag nanoparticles with SBS	52%	Yes	19.5	$f_0 \approx 2.2$ GHz	–	[42]
Graphene sheet	–	–	65@500 nm	0.46–0.52 GHz	–	[43]
Carbon nanotube	–	No	10@350 nm	1.5–2 GHz	–	[15]
Monolayer graphene/AgNW network	75%@100 nm	Yes	6@100 nm	5.6–12.8 GHz	Yes	This work

Note: f_0: Resonance frequency.

spectroscopy (Perkin-Elmer Lambda 950 spectrophotometer), a four-probe resistance measuring meter (Guangzhou 4-probe Tech Co. Ltd., RTS-4) and Raman spectroscopy (Horiba HR800 Raman system with a 514 nm laser wavelength).

Laser Cutting of Antenna Pattern: The system used was a Universal PLS 6MW with a 50 W CO_2 laser. During the cutting process, the laser power was 3.0%, and the related speed was 16%. For each pattern, the laser was used to cut twice in succession to improve the cutting precision.

Electromagnetic Simulations and Numerical Analysis: All electromagnetic simulations and numerical analyses for the graphene-based antennas were performed using a high-frequency structure simulator (Ansoft HFSS) based on the finite element method and Agilent ADS, respectively. In the simulations, the flexible substrate had a dielectric constant of 3.9 and a low profile of $d = 0.125$ mm. The sheet resistance of the graphene/AgNW was measured as $R_s = 6\ \Omega\ sq^{-1}$ using the four-probe method, and the thickness of 100 nm was measured by SEM. Furthermore, the RFID antennas were designed in the simulation to match the impedance of the actual tag chip (RLT111G7, provided by Ray-Links Corp.).

Antenna Measurement: Antennas were bonded to subminiature version A (SMA) connectors with a typical impedance of 50 Ω and connected to a network analyzer (Agilent PNA-X series N5242A).

The graphene/AgNW-based antenna under test and the reference radiating antenna were connected with the VNA. The graphene/AgNW-based antenna was placed on a turntable as a receiver, and the standard reference antenna was fastened on a stand as a radiator. The data were recorded for every 5° rotation.

The reflection coefficient was measured with an Agilent PNA-X series N5242A network analyzer, and the radiation patterns were obtained in an anechoic chamber.

Manufacture of Graphene-Based RFID tag: RFID antennas were also cut using the laser (see Laser cutting of antenna pattern), and RFID chips (RLT111G7) were obtained from Ray-Links Corp. The work of connecting the RFID antennas and chips was done with elargol by Ray-Links Corp.

Supporting Information

Supporting Information is available from the Wiley Online Library or from the author.

Acknowledgements

X.S. and H.L. contributed equally to this work. The authors thank Zhizhen Zhao and Dr. Youfan Hu of Peking University for helping in the antenna laser cutting. This work was financially supported by the Beijing Municipal Science and Technology Commission (Nos. Z181100004818004, Z181100001018029), National Natural Science Foundation of China (Nos. 51432002, 51520105003, 51861145202, 61574083 and 61434001), National Basic Research Program of China (Nos. 2016YFA0200103 and 2015CB352101), National Key R&D Program (No. 2016YFA0200400), Open Research Fund Program of the State Key Laboratory of Low-Dimensional Quantum Physics (No. KF201715), and Foshan-Tsinghua Innovation Special Fund (FTISF) (No. 2018THFS0415).

Conflict of Interest

The authors declare no conflict of interest.

Keywords

flexible and transparent wireless electronics, graphene, radio frequency, synergistic effects

Received: November 22, 2019
Revised: January 9, 2020
Published online: February 13, 2020

[1] J. Park, S. Y. Lee, J. Kim, D. Park, W. Choi, W. Hong, *IEEE Trans. Antennas Propag.* **2019**, *67*, 2942.
[2] J. Park, J. Kim, S.-Y. Kim, W. H. Cheong, J. Jang, Y.-G. Park, K. Na, Y.-T. Kim, J. H. Heo, C. Y. Lee, *Sci. Adv.* **2018**, *4*, eaap9841.
[3] J. Kim, M. Kim, M. S. Lee, K. Kim, S. Ji, Y. T. Kim, J. Park, K. Na, K. H. Bae, H. K. Kim, F. Bien, C. Y. Lee, J. U. Park, *Nat. Commun.* **2017**, *8*, 14997.
[4] J. Kim, A. S. Campbell, B. E. de Avila, J. Wang, *Nat. Biotechnol.* **2019**, *37*, 389.

[5] L. Zhou, M. Yu, X. Chen, S. Nie, W.-Y. Lai, W. Su, Z. Cui, W. Huang, *Adv. Funct. Mater.* **2018**, *28*, 1705955.
[6] Y. Yang, S. Jeong, L. Hu, H. Wu, S. W. Lee, Y. Cui, *Proc. Natl. Acad. Sci. USA* **2011**, *108*, 13013.
[7] S. Lee, K. Lee, C. H. Liu, G. S. Kulkarni, Z. Zhong, *Nat. Commun.* **2012**, *3*, 1018.
[8] Z. N. Low, J. H. Cheong, C. L. Law, *IEEE Antennas Wireless Propag. Lett.* **2005**, *4*, 237.
[9] H. H. Lee, K. S. Chou, K. C. Huang, *Nanotechnology* **2005**, *16*, 2436.
[10] Alien Technology, ALN-9610 Squig Inlay, http://www.alientechnology.com/wp-content/uploads/ALN-9610%20Squig%20Higgs3%20(2015-12-18).pdf. (accessed: August 2019).
[11] Y. Su, X. Ping, K. J. Yu, J. W. Lee, J. A. Fan, B. Wang, M. Li, R. Li, D. V. Harburg, Y. Huang, C. Yu, S. Mao, J. Shim, Q. Yang, P. Y. Lee, A. Armonas, K. J. Choi, Y. Yang, U. Paik, T. Chang, T. J. Dawidczyk, Y. Huang, S. Wang, J. A. Rogers, *Adv. Mater.* **2017**, *29*, 1604989.
[12] D. Tang, Q. Wang, Z. Wang, Q. Liu, B. Zhang, D. He, Z. Wu, S. Mu, *Sci. Bull.* **2018**, *63*, 574.
[13] N. J. Kirsch, N. A. Vacirca, E. E. Plowman, T. P. Kurzweg, A. K. Fontecchio, K. R. Dandekar, in *Proc. of the 2009 IEEE Int. Conf. on RFID*, IEEE, Piscataway, NJ **2009**, pp. 278–282, https://ieeexplore.ieee.org/document/4911205.
[14] N. A. Vacirca, J. K. McDonough, K. Jost, Y. Gogotsi, T. P. Kurzweg, *Appl. Phys. Lett.* **2013**, *103*, 073301.
[15] I. Puchades, J. E. Rossi, C. D. Cress, E. Naglich, B. J. Landi, *ACS Appl. Mater. Interfaces* **2016**, *8*, 20986.
[16] C. Rutherglen, D. Jain, P. Burke, *Nat. Nanotechnol.* **2009**, *4*, 811.
[17] K. Pan, Y. Fan, T. Leng, J. Li, Z. Xin, J. Zhang, L. Hao, J. Gallop, K. S. Novoselov, Z. Hu, *Nat. Commun.* **2018**, *9*, 5197.
[18] X. Huang, T. Leng, M. Zhu, X. Zhang, J. Chen, K. Chang, M. Aqeeli, A. K. Geim, K. S. Novoselov, Z. Hu, *Sci. Rep.* **2015**, *5*, 18298.
[19] A. Scidà, S. Haque, E. Treossi, A. Robinson, S. Smerzi, S. Ravesi, S. Borini, V. Palermo, *Mater. Today* **2018**, *21*, 223.
[20] H. Y. Chang, M. N. Yogeesh, R. Ghosh, A. Rai, A. Sanne, S. Yang, N. Lu, S. K. Banerjee, D. Akinwande, *Adv. Mater.* **2016**, *28*, 1818.
[21] A. Sarycheva, A. Polemi, Y. Liu, K. Dandekar, B. Anasori, Y. Gogotsi, *Sci. Adv.* **2018**, *4*, eaau0920.
[22] R. R. Nair, P. Blake, A. N. Grigorenko, K. S. Novoselov, T. J. Booth, T. Stauber, N. M. R. Peres, A. K. Geim, *Science* **2008**, *320*, 1308.
[23] J.-H. Chen, C. Jang, S. Xiao, M. Ishigami, M. S. Fuhrer, *Nat. Nanotechnol.* **2008**, *3*, 206.
[24] C. Lee, X. Wei, J. W. Kysar, J. Hone, *Science* **2008**, *321*, 385.
[25] A. K. Geim, K. S. Novoselov, *Nat. Mater.* **2007**, *6*, 183.
[26] J. S. Bunch, S. S. Verbridge, J. S. Alden, A. M. van der Zande, J. M. Parpia, H. G. Craighead, P. L. McEuen, *Nano Lett.* **2008**, *8*, 2458.
[27] S. Hu, M. Lozada-Hidalgo, F. Wang, A. Mishchenko, F. Schedin, R. Nair, E. Hill, D. Boukhvalov, M. Katsnelson, R. Dryfe, I. V. Grigorieva, H. A. Wu, A. K. Geim, *Nature* **2014**, *516*, 227.
[28] B. Deng, P. C. Hsu, G. Chen, B. N. Chandrashekar, L. Liao, Z. Ayitimuda, J. Wu, Y. Guo, L. Lin, Y. Zhou, M. Aisijiang, Q. Xie, Y. Cui, Z. Liu, H. Peng, *Nano Lett.* **2015**, *15*, 4206.
[29] X. Sun, L. Lin, L. Sun, J. Zhang, D. Rui, J. Li, M. Wang, C. Tan, N. Kang, D. Wei, H. Q. Xu, H. Peng, Z. Liu, *Small* **2018**, *14*, 1702916.
[30] L. M. Malard, M. A. Pimenta, G. Dresselhaus, M. S. Dresselhaus, *Phys. Rep.* **2009**, *473*, 51.
[31] Z. Ni, Y. Wang, T. Yu, Z. Shen, *Nano Res.* **2008**, *1*, 273.
[32] X. Y. Zeng, Q. K. Zhang, R. M. Yu, C. Z. Lu, *Adv. Mater.* **2010**, *22*, 4484.
[33] A. F. Molisch, *Wireless Communications*, Wiley, Hoboken, NJ, USA **2012**.
[34] K. Maize, S. R. Das, S. Sadeque, A. M. S. Mohammed, A. Shakouri, D. B. Janes, M. A. Alam, *Appl. Phys. Lett.* **2015**, *106*, 143104.
[35] S. H. Choi, J. K. Park, S. K. Kim, J. Y. Park, *Microwave Opt. Technol. Lett.* **2004**, *40*, 399.
[36] W. L. Stutzman, G. A. Thiele, *Antenna Theory and Design*, Wiley, Hoboken, NJ, USA **2013**.
[37] M. Kaur, M. Sandhu, N. Mohan, P. S. Sandhu, *Int. J. Comput. Electr. Eng.* **2011**, *3*, 151.
[38] J. Zhang, G. Tian, A. Marindra, A. Sunny, A. Zhao, *Sensors* **2017**, *17*, 265.
[39] G. Marrocco, *IEEE Antennas Propag. Mag.* **2008**, *50*, 66.
[40] X. Huang, T. Leng, K. H. Chang, J. C. Chen, K. S. Novoselov, Z. Hu, *2D Mater.* **2016**, *3*, 025021.
[41] S. Kosuga, R. Suga, O. Hashimoto, S. Koh, *Appl. Phys. Lett.* **2017**, *110*, 233102.
[42] M. Park, J. Im, M. Shin, Y. Min, J. Park, H. Cho, S. Park, M.-B. Shim, S. Jeon, D.-Y. Chung, *Nat. Nanotechnol.* **2012**, *7*, 803.
[43] K. Y. Shin, J. Y. Hong, J. Jang, *Adv. Mater.* **2011**, *23*, 2113.